Editors' Suggestion

Metasurfaces with Maximum Chirality Empowered by Bound States in the Continuum

Maxim V. Gorkunov,[1] Alexander A. Antonov,[1] and Yuri S. Kivshar[2]
[1]Shubnikov Institute of Crystallography of the Federal Scientific Research Centre "Crystallography and Photonics," Russian Academy of Science, Moscow 119333, Russia
[2]Nonlinear Physics Centre, Research School of Physics, Australian National University, Canberra ACT 2601, Australia

(Received 28 June 2020; accepted 6 August 2020; published 27 August 2020)

We demonstrate that rotationally symmetric chiral metasurfaces can support sharp resonances with the maximum optical chirality determined by precise shaping of bound states in the continuum (BICs). Being uncoupled from one circular polarization of light and resonantly coupled to its counterpart, a metasurface hosting the chiral BIC resonance exhibits a narrow peak in the circular dichroism spectrum with the quality factor limited by weak dissipation losses. We propose a realization of such chiral BIC metasurfaces based on pairs of dielectric bars and validate the concept of maximum chirality by numerical simulations.

DOI: 10.1103/PhysRevLett.125.093903

Chirality refers to a global property of many systems which do not coincide with their mirror images [1]. Photonic structures made of chiral elements exhibit chiroptical effects such as optical dichroism for left and right circularly polarized light, the property highly suitable for chiral nanophotonics [2]. However, strong chiroptical effects are challenging to achieve, and strong resonances of plasmonic structures [3] have been suggested for chiral mirrors [4,5]. Intrinsic chirality, i.e., chiroptical effects at normal incidence, is prohibited in planar structures but can be observed in opaque metallic structures of complex shapes [6] and dielectric layers facilitating chiral excitation of higher-order multipoles [7].

Recently, all-dielectric metasurfaces have been employed to achieve sharp optical resonances empowered by the physics of bound states in the continuum (BICs) when light at the resonance remains localized in the metasurface even though the state coexists with a continuum of electromagnetic waves [8–10]. In practice, BICs are realized with high but finite quality factors due to structural losses and imperfections, and they are usually termed quasi-BICs. The BIC-inspired resonances in the symmetry-broken all-dielectric metasurfaces are receiving attention for many applications [11–13]. To date, all metasurfaces supporting quasi-BIC resonances were associated with the interaction of BICs and radiative continuum due to in-plane symmetry breaking. Combined in twisted stacks such metasurfaces can remarkably efficiently control the chirality and spectrum of reflected light [14]. However, the potential of direct chirality manipulation using out-of-plane BIC symmetry breaking remains unexplored.

In this Letter, we introduce the concept of highly transparent chiral metasurfaces by shaping BICs into quasi-BICs of maximum optical chirality delivering narrow peak of unit height in the circular dichroism (CD) spectrum. We propose a design based on dimers of dielectric bars and validate the maximum chirality of its quasi-BIC resonance by numerical modeling.

We consider a metasurface shown schematically in Fig. 1, located in the xy plane with the z axis being the Nth order rotational symmetry axis (C_N symmetry group). For $N \geq 3$, all polarization transformations of incoming waves incident normally from both sides are determined by the chirality. Assuming $e^{-i\omega t}$ time dependence of all fields, we consider waves polarized along the complex unit vectors:

$$\mathbf{e}_{\pm} = (\mathbf{e}_x \mp i\mathbf{e}_y)/\sqrt{2}. \tag{1}$$

For waves propagating in the positive z direction, $\mathbf{e}_+$ and $\mathbf{e}_-$ correspond to the right circular polarization (RCP) and left circular polarization (LCP), respectively. For waves in the negative z direction, the opposite is true.

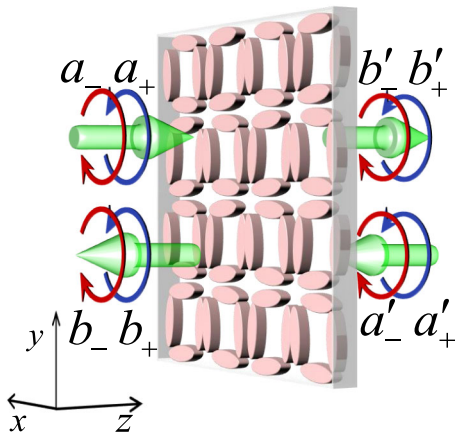

FIG. 1. Sketch of the transmission-reflection problem for rotationally symmetric chiral metasurfaces described by the S-matrix Eq. (2).

Most generally, this transmission-reflection problem is described by an S-matrix equation (see the Supplemental Material [15]) relating the outgoing wave amplitudes, $b_\pm$ and $b'_\pm$, with the incident wave amplitudes, $a_\pm$ and $a'_\pm$:

$$\begin{pmatrix} b_+ \\ b'_+ \\ b_- \\ b'_- \end{pmatrix} = \begin{pmatrix} r & t_L & 0 & 0 \\ t_R & r' & 0 & 0 \\ 0 & 0 & r & t_R \\ 0 & 0 & t_L & r' \end{pmatrix} \begin{pmatrix} a_+ \\ a'_+ \\ a_- \\ a'_- \end{pmatrix}. \tag{2}$$

Fundamental principle of reciprocity together with the rotational symmetry put substantial restrictions on the metasurface transmission and reflection [22,23]. In particular, the RCP and LCP transmission amplitudes, t_R and t_L, respectively, are equal for both sides of incidence along with the key optical parameters, optical rotation (OR) and CD:

$$\mathrm{OR} = \frac{1}{2}(\arg t_L - \arg t_R), \qquad \mathrm{CD} = \frac{|t_R|^2 - |t_L|^2}{|t_R|^2 + |t_L|^2}. \tag{3}$$

The reciprocity also determines that the reflection amplitudes r and r' are helicity independent, which directly relates the CD with the energy dissipation. Indeed, absorbed parts of the energy of incident RCP or LCP waves, $A_{R,L} = 1 - |t_{R,L}|^2 - |r|^2$, determine that the transmittance difference $|t_R|^2 - |t_L|^2 = A_L - A_R$ arises due to a difference in dissipation.

The inherent connection of the CD with dissipation naturally determines a quantitative condition of maximum optical chirality: it is achieved when the metasurface is fully transparent for one circular polarization and totally absorbs its counterpart. Note that this excludes conversion of wave helicity and the metasurface is dual [24].

To specify a feasible route to the maximum chirality, we employ the phenomenological coupled-mode theory (CMT) allowing expressing abstract scattering amplitudes in terms of physically meaningful parameters [25–27]. CMT generalized for chiral metasurfaces with plasmon [22] and dielectric [28] resonances reproduced their observed strong chirality and clarified its origin.

In CMT, transmission and reflection are split into background and resonant channels with the latter determined by excitation and irradiation of eigenstates hosted by the structure. Note that particular eigenstate normalization is not required [27]. CMT yields (see these and following relations derived in Supplemental Material [15]) the following transmission amplitudes:

$$t_R = \tau - \frac{m_+ m'_-}{i(\omega - \omega_0) - \gamma_0}, \qquad t_L = \tau - \frac{m'_+ m_-}{i(\omega - \omega_0) - \gamma_0}, \tag{4}$$

where τ is the background transmission amplitude, the resonance frequency ω_0 and damping γ_0 are helicity independent, and $m_\pm$ are the parameters of coupling of the eigenstates to the waves of corresponding helicity incident on one metasurface side, and $m'_\pm$ are those for the other side. Accordingly, the optical chirality (3) is determined by the chirality of eigenstate coupling to the free-space continuum.

All losses contribute to the damping $\gamma_0 = \gamma_d + \gamma_r$, where γ_d is its dissipative part, and the radiative part is determined by the coupling:

$$2\gamma_r = |m_+|^2 + |m'_+|^2 = |m_-|^2 + |m'_-|^2. \tag{5}$$

The difference of transmittances is expressed as

$$|t_R|^2 - |t_L|^2 = 2\gamma_d \frac{|m_-|^2 - |m_+|^2}{(\omega - \omega_0)^2 + (\gamma_r + \gamma_d)^2}, \tag{6}$$

which emphasizes the crucial role of dissipation for the CD.

Consider, for definiteness, how to maximize the optical chirality by enhancing $|t_R|$ and suppressing $|t_L|$. Equation (4) suggests achieving the ultimate value $|t_R| = 1$ by setting $|\tau| = 1$ and $m_+ m'_- = 0$. The latter condition requires uncoupling the eigenstate from waves of certain helicity on a particular metasurface side.

For example, we set $m_+ = 0$ and, according to (6),

$$|t_L|^2 = 1 - 2\gamma_d \frac{|m_-|^2}{(\omega - \omega_0)^2 + (\gamma_r + \gamma_d)^2}, \tag{7}$$

with the minimum reached at the resonance, $\omega = \omega_0$:

$$\min |t_L|^2 = 1 - \frac{8\gamma_d |m_-|^2}{(|m_-|^2 + |m'_-|^2 + 2\gamma_d)^2}, \tag{8}$$

where the radiative damping (5) is substituted. The ultimate limit $\min |t_L|^2 = 0$ is achieved only if simultaneously $m'_- = 0$ and $|m_-|^2 = 2\gamma_d$.

Therefore, the maximum chirality requires $m_+ = m'_- = 0$, i.e., eigenstates selectively decoupled from the free-space continuum. The second condition reduces by Eq. (5) to

$$\gamma_r = \gamma_d \tag{9}$$

which is a classical critical coupling regime [29] of a resonator receiving from the continuum exactly the amount of energy it is capable to dissipate.

To summarize, CMT unambiguously points out that for the maximum optical chirality a metasurface has to do the following: (i) host eigenstates selectively coupled to circularly polarized waves (e.g., the "+" state uncoupled from RCP waves incident on one side and the "−" state uncoupled from RCP waves incident on the other side) and (ii) fully absorb the light of the opposite circular polarization in the critical coupling regime.

Note that the phenomenological approach requires a metasurface performing identically from its both sides, e.g., being coupled with $m_+ = 0$ and $|m_-|^2 = 2\gamma_d$ to the waves on one side and with $m'_- = 0$ and $|m'_+|^2 = 2\gamma_d$ on the other side. This can be ensured by restricting to flipping-symmetric designs having an in-plane C_2 rotational axis.

Achieving maximum optical chirality requires precise control of the coupling of eigenstates to the free-space continuum. In the following, we present a step-by-step design of such eigenstates starting from fully uncoupled BICs and carefully enabling their selective coupling by symmetry breaking perturbations.

Consider a planar lattice of pairs of parallel dielectric bars shown in Fig. 2(a). The lattice is reflection symmetric with respect to three types of mirror planes: those indicated as σ_1 and σ_2 and the plane of drawing. All dimers are in perfectly symmetric situations as the vertical C_2 axes (intersection of planes σ_1 and σ_2) pierce exactly through their centers. All resonant eigenstates transform according to the irreducible representations of the C_2 group and, among those, there is a symmetric A representation. The electric resonance of this symmetry is described by a pair of antiparallel dipole moments $\mathbf{p}_1 = -\mathbf{p}_2$ shown on the top of Fig. 2(a).

To estimate the eigenstate coupling to a plane wave polarized along a unit vector $\mathbf{e}$ and having a wave vector $\mathbf{k}$

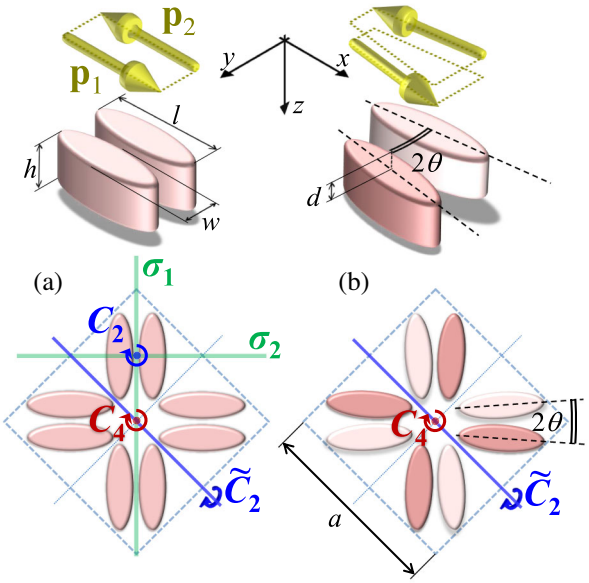

FIG. 2. Shaping quasi-BIC chirality by symmetry breaking. (a) A dimer of parallel bars and their lattice hosting BIC resonances. (b) A dimer of bars vertically offset by d and rotated by θ, and a unit cell of their lattice hosting chiral quasi-BIC resonances. All bars are identical and the colors indicate location on different levels. Two types of mirror symmetry planes and three types of rotational symmetry axes are indicated. The lattice constant a is shown in (b). Relative orientation and offset of electric dipole moments characterizing BIC and quasi-BIC eigenstates are shown on the top for each dimer type.

along the z axis, one can integrate the incident wave field with the eigenstate field or, equivalently, with its current density [11,27]:

$$m_{\mathbf{e}} \propto \int_{V_1,V_2} d\mathbf{r}[\mathbf{j}(\mathbf{r}) \cdot \mathbf{e}]e^{ikz}, \tag{10}$$

where $V_{1,2}$ are the volumes of dielectric bars. For each volume, the integral yields the dipole moment of the corresponding bar, and the antiparallel dipole eigenstate is uncoupled of all incident polarizations as

$$m_{\mathbf{e}} \propto \mathbf{p}_1 \cdot \mathbf{e} + \mathbf{p}_2 \cdot \mathbf{e} = 0. \tag{11}$$

This is a perfect BIC with respect to all normally incident waves.

Introducing weak symmetry breaking transforms BIC into quasi-BIC. As has been studied in detail [11], diverging the bars in plane by an angle θ eliminates the mirror symmetry plane σ_2 and the dimer rotational axis C_2. The parameters of coupling to circularly polarized waves obtained from Eq. (10) with $\mathbf{e} = \mathbf{e}_\pm$ and the dipole moments diverged by θ are

$$m_\pm \propto \mathbf{p}_1 \cdot \mathbf{e}_\pm + \mathbf{p}_2 \cdot \mathbf{e}_\pm = i\sqrt{2}p \sin\theta. \tag{12}$$

They are achiral, as the structure retains two mirror planes: σ_1 and that of the drawing.

An out-of-plane symmetry breaking can be introduced by a small vertical offset d of bars within each dimer eliminating the mirror plane σ_1 together with the dimer C_2 axis. The corresponding coupling parameters,

$$m_\pm \propto \mathbf{p}_1 \cdot \mathbf{e}_\pm + \mathbf{p}_2 \cdot \mathbf{e}_\pm e^{ikd} = i\sqrt{2}pe^{ikd/2} \sin kd/2, \tag{13}$$

are also achiral due to the remaining mirror plane σ_2.

Combining the offset by d with the rotation by θ, as illustrated in Fig. 2(b), breaks all mirror symmetries. Depicted square lattice of the dimers possesses the out-of-plane C_4 and the in-plane $\tilde{C}_2$ rotational axes. The coupling parameters estimated as $m_\pm \propto \mathbf{p}_1 \cdot \mathbf{e}_\pm + \mathbf{p}_2 \cdot \mathbf{e}_\pm e^{ikd} = i\sqrt{2}pe^{ikd/2} \sin(kd/2 \mp \theta)$, elucidate the rise of optical chirality. The retained $\tilde{C}_2$ axis ensures similar coupling to waves on the other side: $m'_\pm \propto i\sqrt{2}pe^{ikd/2} \times \sin(kd/2 \pm \theta)$.

Remarkably, maximizing the quasi-BIC chirality is possible by a simple adjustment of the offset and rotation as

$$\theta = kd/2, \tag{14}$$

which ensures that $m_+ = m'_- = 0$. Under this condition, the remaining coupling parameters

$$m_- = m'_+ \propto i\sqrt{2}pe^{i\theta} \sin(2\theta) \tag{15}$$

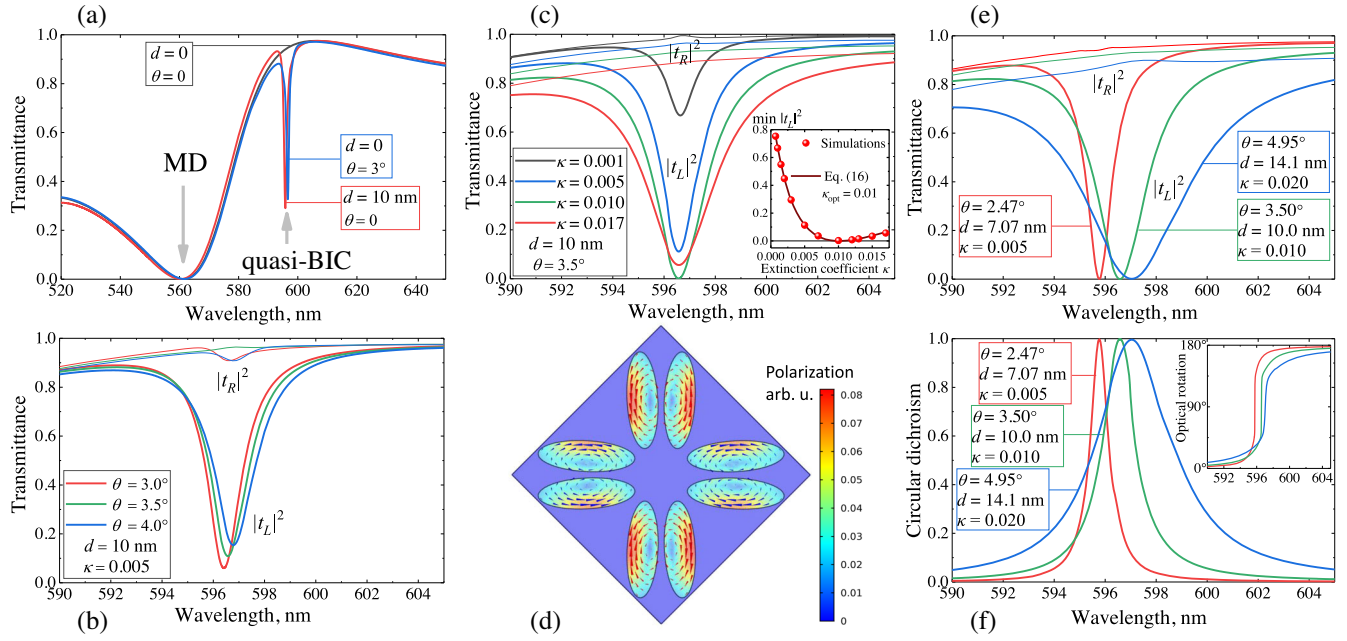

FIG. 3. Simulated transformation of BIC into maximum chiral quasi-BIC. Transmittance spectra of achiral structures (a) comprised of parallel bar dimers, dimers rotated by θ and dimers offset by d, exhibit strong MD resonance and sharp quasi-BIC resonance controlled by rotation and offset. RCP and LCP transmittance spectra (b) of chiral structures with equal offset and different rotation angles. RCP and LCP transmittance spectra (c) of structures with quasi-BIC uncoupled from RCP waves for different extinction coefficient κ with the inset comparing simulated minimum transmittance with that predicted by CMT Eq. (16). Polarization distribution (d) in maximum chiral quasi-BIC for $\kappa = 0.01$, $\theta = 3.5°$, and $d = 10$ nm excited by linearly polarized light of $\lambda = 596.5$ nm: distribution of real (red cones) and imaginary (blue cones) polarization vector components are juxtaposed with the colormap of average polarization. Spectra of transmittances (e), CD (f), and OR [inset in (f)] of structures hosting maximum chiral quasi-BICs with symmetry breaking parameters and losses following the scaling rule $\theta^2 \propto d^2 \propto \kappa$.

are controlled by θ and allow continuous tuning to match the dissipation in the critical coupling regime (9).

To validate the symmetry-based analysis, we numerically study a particular structure using COMSOL MULTIPHYSICS. To keep relevance with available materials (silicon and germanium), we model bars consisting of dielectric having complex refractive index $n = 4 + i\kappa$ with small extinction coefficient κ. For simplicity, the background refractive index is set to unity. The dimensions of elliptical bars are $l = 220$ nm, $w = 70$ nm, and $h = 100$ nm (see Fig. 2). The gap between parallel bars is set to 15 nm and the square lattice constant $a = 480$ nm excludes diffraction in the considered wavelength range.

First, we simulate the transmission of normally incident light by achiral lattices of parallel bar dimers, dimers diverged by an in-plane rotation by $\theta = 3°$, and dimers with an out-of-plane offset $d = 10$ nm. In all three cases, the transmission is polarization insensitive. As seen in Fig. 3(a), the transmittance spectra stay generally very close exhibiting a broad minimum at about the 560 nm wavelength associated with the magnetic-dipole (MD) resonance. Close to the 596 nm wavelength, either of the two weak symmetry perturbations give rise to much sharper quasi-BIC resonances fully inline with the estimates (11)–(13).

To determine the parameters necessary for a quasi-BIC uncoupled from RCP waves, we use Eq. (14) to estimate that the offset $d = 10$ nm at a 596 nm wavelength requires the angle $\theta = 3.0°$. Indeed, as shown in Fig. 3(b), for this angle, the resonance of the RCP transmittance is weak. However, the ideal uncoupling occurs for $\theta = 3.5°$. Further increasing the angle to $\theta = 4.0°$ restores the resonance. We conclude that Eq. (14) specifies geometries very close to optimal, though a small mismatch arises due to a slight misalignment of the bar dipole moment and shape.

Knowing the perfect combination of θ and d, we proceed to verify the main CMT conclusions. For a proper chiral q-BIC state isolated from RCP waves by $m_+ = m'_- = 0$, the minimum LCP transmittance at the resonance is given by Eq. (8) with $m'_- = 0$. The remaining coupling parameter $|m_-|^2$ is determined by the bar refractive index, dimensions and packing, while weak dissipation affects it negligibly. The damping, on the contrary, is determined by the dissipation, as $\gamma_d \propto \kappa$.

If a certain value $\kappa = \kappa_{\text{opt}}$ corresponds to the critical coupling regime, then Eq. (8) can be expressed as

$$\min |t_L|^2 = \left(\frac{\kappa_{\text{opt}} - \kappa}{\kappa_{\text{opt}} + \kappa}\right)^2. \tag{16}$$

Accordingly, we keep all other parameters fixed and simulate the transmission of structures with different κ, as illustrated in Fig. 3(c). Decreasing κ drastically elevates the $|t_L|^2$ minimum as the losses are critical for the CD. Increasing κ far above 0.01 also negatively affects CD, elevates the $|t_L|^2$ minimum and suppresses $|t_R|^2$. Plotting $\min|t_L|^2$ values as a function of κ and fitting them by the simple dependence (16) [see the inset in Fig. 3(c)] validates the CMT conclusions and precisely determines $\kappa_{\mathrm{opt}} = 0.01$. The inner structure of the chiral quasi-BIC state is illustrated in Fig. 3(d) by the polarization distribution within a metasurface unit cell upon linearly polarized illumination. Only the LCP part interacts with the chiral quasi-BIC and excites the currents of the $\mathbf{e}_-$ symmetry: anticlockwise rotation by $\pi/2$ is equivalent to multiplication by i.

Finally, combining Eqs. (15) and (14) reveals a general rule: the maximum chirality is established with the three small parameters scaling as $\theta^2 \propto d^2 \propto \kappa$. To verify this, we simulate the transmission of structures with doubled and halved κ and with θ and d varied accordingly by a factor of $\sqrt{2}$. As shown in Fig. 3(e), the structures indeed host quasi-BICs with maximal chirality; their CD spectra in Fig. 3(f) possess resonances of unit height accompanied by typical OR kinks shown in the inset.

As the Si refractive index at $\lambda = 595$ nm is $n_{\mathrm{Si}} = 3.948 + 0.021i$ [30], the broader resonance in Figs. 3(e) and 3(f) describes a practically available realization. Lower extinction coefficients of 0.01 and 0.005 correspond to Si at ~700 nm and ~800 nm, respectively. Sharper CD resonances available in the near IR range require fabrication technique supporting precise nanometer-scale offsets.

In conclusion, we have developed the concept of chiral BIC metasurfaces transmitting one circular polarization and resonantly blocking the opposite polarization. Our design strategy is applicable for maximizing the optical chirality of other types of resonant metasurfaces operating in the visible and near IR spectral ranges.

The work of M. V. G. and A. A. A. is supported by the Ministry of Science and Higher Education of the Russian Federation within the State assignment of FSRC "Crystallography and Photonics" RAS. Y. S. K. acknowledges a support from the Strategic Fund of the Australian National University. The authors are grateful to Alexey Kondratov for his assistance with COMSOL MULTIPHYSICS modeling.

[1] W. Kelvin, *The Molecular Tactics of a Crystal*, Robert Boyle Lecture (Clarendon Press, Oxford, 1894).
[2] M. Schäferling, *Chiral Nanophotonics* (Springer International Publishing, Switzerland, 2017).
[3] S. S. Oh and O. Hess, Chiral metamaterials: Enhancement and control of optical activity and circular dichroism, Nano Convergence **2**, 24 (2015).
[4] E. Plum and N. I. Zheludev, Chiral mirrors, Appl. Phys. Lett. **106**, 221901 (2015).
[5] M. Hentschel, M. Schäferling, X. Duan, H. Giessen, and N. Liu, Chiral plasmonics, Sci. Adv. **3**, e1602735 (2017).
[6] M. V. Gorkunov, A. A. Ezhov, V. V. Artemov, O. Y. Rogov, and S. G. Yudin, Extreme optical activity and circular dichroism of chiral metal hole arrays, Appl. Phys. Lett. **104**, 221102 (2014).
[7] A. Y. Zhu, W. T. Chen, A. Zaidi, Y.-W. Huang, M. Khorasaninejad, V. Sanjeev, C.-W. Qiu, and F. Capasso, Giant intrinsic chiro-optical activity in planar dielectric nanostructures, Light Sci. Appl. **7**, 17158 (2017).
[8] C. W. Hsu, B. Zhen, A. D. Stone, J. D. Joannopoulos, and M. Soljačić, Bound states in the continuum, Nat. Rev. Mater. **1**, 16048 (2016).
[9] E. N. Bulgakov and A. F. Sadreev, Transfer of spin angular momentum of an incident wave into orbital angular momentum of the bound states in the continuum in an array of dielectric spheres, Phys. Rev. A **94**, 033856 (2016).
[10] K. Koshelev, A. Bogdanov, and Y. Kivshar, Meta-optics and bound states in the continuum, Sci. Bull. **64**, 836 (2019).
[11] K. Koshelev, S. Lepeshov, M. Liu, A. Bogdanov, and Y. Kivshar, Asymmetric Metasurfaces with High-Q Resonances Governed by Bound States in the Continuum, Phys. Rev. Lett. **121**, 193903 (2018).
[12] F. Yesilkoy, E. R. Arvelo, Y. Jahani, M. Liu, A. Tittl, V. Cevher, Y. Kivshar, and H. Altug, Ultrasensitive hyperspectral imaging and biodetection enabled by dielectric metasurfaces, Nat. Photonics **13**, 390 (2019).
[13] K. Koshelev, Y. Tang, K. Li, D.-Y. Choi, G. Li, and Y. Kivshar, Nonlinear metasurfaces governed by bound states in the continuum, ACS Photonics **6**, 1639 (2019).
[14] A. Overvig, N. Yu, and A. Alu, Chiral quasi-bound states in the continuum, arXiv:2006.05484.
[15] See the Supplemental Material at http://link.aps.org/supplemental/10.1103/PhysRevLett.125.093903 for the analysis of S-matrix symmetry and derivation of Eq. (2), as well as for a rigorous formulation of CMT yielding Eqs. (4)–(6), which includes Refs. [16–21].
[16] J. Mur-Petit and R. A. Molina, Chiral bound states in the continuum, Phys. Rev. B **90**, 035434 (2014).
[17] C.-K. Chiu, J. C. Teo, A. P. Schnyder, and S. Ryu, Classification of topological quantum matter with symmetries, Rev. Mod. Phys. **88**, 035005 (2016).
[18] C. Hermann, Tensoren und Kristallsymmetrie, Z. Kristallogr. Cryst. Mater. **89**, 32 (1934).
[19] B. Hopkins, A. N. Poddubny, A. E. Miroshnichenko, and Y. S. Kivshar, Circular dichroism induced by Fano resonances in planar chiral oligomers, Laser Photonics Rev. **10**, 137 (2015).
[20] Z. F. Sadrieva, M. A. Belyakov, M. A. Balezin, P. V. Kapitanova, E. A. Nenasheva, A. F. Sadreev, and A. A. Bogdanov, Experimental observation of a symmetry-protected bound state in the continuum in a chain of dielectric disks, Phys. Rev. A **99**, 053804 (2019).
[21] Z.Hu, L. Yuan, and Y. Y. Lu, Bound states with complex frequencies near the continuum on lossy periodic structures, Phys. Rev. A **101**, 013806 (2020).
[22] A. V. Kondratov, M. V. Gorkunov, A. N. Darinskii, R. V. Gainutdinov, O. Y. Rogov, A. A. Ezhov, and V. V. Artemov,

Extreme optical chirality of plasmonic nanohole arrays due to chiral Fano resonance, Phys. Rev. B **93**, 195418 (2016).

[23] M. V. Gorkunov, V. E. Dmitrienko, A. A. Ezhov, V. V. Artemov, and O. Y. Rogov, Implications of the causality principle for ultra chiral metamaterials, Sci. Rep. **5**, 9273 (2015).

[24] I. Fernandez-Corbaton, M. Fruhnert, and C. Rockstuhl, Objects of Maximum Electromagnetic Chirality, Phys. Rev. X **6**, 031013 (2016).

[25] S. Fan, W.Suh, and J. D. Joannopoulos, Temporal coupled-mode theory for the Fano resonance in optical resonators, J. Opt. Soc. Am. A **20**, 569 (2003).

[26] J. W. Yoon, M. J. Jung, S. H. Song, and R. Magnusson, Analytic theory of the resonance properties of metallic nanoslit arrays, IEEE J. Quantum Electron. **48**, 852 (2012).

[27] F. Alpeggiani, N. Parappurath, E. Verhagen, and L. Kuipers, Quasinormal-Mode Expansion of the Scattering Matrix, Phys. Rev. X **7**, 021035 (2017).

[28] M. V. Gorkunov, O. Y. Rogov, A. V. Kondratov, V. V. Artemov, R. V. Gainutdinov, and A. A. Ezhov, Chiral visible light metasurface patterned in monocrystalline silicon by focused ion beam, Sci. Rep. **8**, 11623 (2018).

[29] H. A. Haus, *Waves and Fields in Optoelectronics* (Prentice-Hall, Englewood Cliffs, NJ, 1984).

[30] G. Jellison, Optical functions of silicon determined by two-channel polarization modulation ellipsometry, Opt. Mater. **1**, 41 (1992).